Simulation of spray formation using secondary atomization and turbulent vaporization models

Emmanuel Bodèle[1], Pierre Pillot[1], Iskender Gökalp[1], Stephan Zurbach[2] and Didier Saucereau[2]

1. Centre National de la Recherche Scientifique
   Laboratoire de Combustion et Systèmes Réactifs
   1c, avenue de la Recherche Scientifique
   45071 Orléans Cedex 2, France
2. SNECMA Moteurs
   Groupe SNECMA
   BP 802 – Forêt de Vernon
   27208 Vernon, France

This paper describes the development of secondary atomization and turbulent vaporization models based on experimental results obtained at Laboratoire de Combustion et Systèmes Réactifs. Experimental results, their use for modeling and their integration in CFD codes (THESEE from SNECMA and MSD from ONERA) are briefly presented. The computations presented in this paper concern the simulation of a single LOX/H_2 cryogenic coaxial injector similar to those used in the Vulcain engine of the European launcher Ariane V. For liquid oxygen, initial conditions are respectively 50g/s and 80K for mass flow rate and tempearture. For hydrogen, initial conditions are respectively 23.7g/s, 287K and 319m/s for mass flow rate, temperature and velocity. In the case of secondary atomization, the results concern the characterization of the final spray in the computational domain (number and size of droplets, mean droplet diameters, droplet locations, spray length,...). In the case of turbulent vaporization, results concern mainly the droplet vaporization rate and the droplet locations.

1. Introduction

The two-phase combustion process is largely influenced by basic phenomena such as atomization and droplet vaporization. The atomization consists in the formation of a spray composed of droplets with various sizes. The formation of such spray is generally decomposed in two more elementary processes. The first step, called primary atomization, consists in the formation of "large" liquid parcels by the action of aerodynamic forces at the jet surface. The second step, called secondary atomization, consists in reduction of the liquid parcel dimensions by successive fragmentations. For a single droplet, the secondary fragmentation is controlled by several parameters and especially by Weber (We) and Reynolds (Re) numbers (Eq. 1):

$$We = \frac{\rho_g \cdot V^2 \cdot D}{\sigma} \, , \, Re = \frac{\rho_g \cdot V \cdot D}{\mu_g} \tag{1}$$

The Weber number is often considered as the main parameter for the secondary atomization [8, 9] and a critical Weber (We_c) is generally defined as We_c=12. Below this value no fragmentation process can be observed. For larger values of Weber number ($We > We_c$), several breakup regimes can be observed. The designation of these regimes depends on authors. One of most complete classification is the Shraiber and al. one [6], in which 8 regimes are described. The transition between breakup regimes is based on the criterion $We/\sqrt{Re}$ previously introduced by Gelfand [2]. The

number and the size of secondary fragments created during a fragmentation is generally dependent on the breakup regime. For the description of the fragmentation phenomenon, different characteristic times are usually considered, like the initiation time (T_{ini}) or total the breakup time (T_{BU}). The initiation time corresponds to the time between the penetration of the droplet into the fragmentation zone and the moment of appearing of the first secondary droplets. In fact, this time is equal to the time of deformation of the initial droplet.
The vaporization of a liquid droplet and in general of a liquid is widely dependant on external conditions and on liquid physical properties. Indeed, an increase of certain parameters such as ambient temperature or relative velocity between gas and droplet results in an increase in vaporization rate. To describe the vaporization of a liquid droplet, several models exist. One of the most usefull is the quasi-steady theory [3, 7], conducting to the following formulation (Eq. 2) for the vaporization law of a single droplet:

$$d^2 = D_0^2 - K_S \cdot t \text{ with } K_S = 8 \cdot \frac{\rho_g}{\rho_L} \cdot D \ln(1+B) \tag{2}$$

where d, K_S, D, and B are respectively the instantaneous diameter, the static vaporization rate, the binary diffusion coefficient and the transfert coefficient (more details can be found in Refs. [1,3,4,7]).

2. Numerical models

2.1. Secondary atomization model

The secondary atomization model is based on the Vieille's experimental studies [4, 8, 9]. The objectives of these experiments were the complete characterization of the secondary atomization process in terms of breakup regimes, breakup initiation time and secondary droplet distributions (number and size of fragments). To observe the fragmentation process, a single liquid oxygen droplet is introduced into a high velocity (up to 30m/s) and high pressure (up to 8MPa) helium flow. The atomization phenomena is followed by high speed video (up to 9000im/s). With this technique, depending on experimental conditions, it was possible to identify 3 breakup regimes, according to the Shraiber and al. classification: the bag breakup, the transitional breakup and the shear breakup. According to the criterion previously introduced by Gelfand [2], the transition between regimes is well reproduced by the following correlation (Eq. 3):

$$\frac{We}{\sqrt{Re}} = C \cdot DR^{0.25} \cdot VR^{-0.5} \tag{3}$$

where DR and VR represent respectively the density and viscosity ratios between the two phases. For the determination of the breakup regime, only the value of the constant C is to be evaluated. From the experiments, values for C are 0.25, 0.5 and 0.7 for the bag, transitional and shear breakup regimes respectively. The dynamic of the atomization is controlled by the breakup initiation time (T_{ini}) previously defined. This time is experimentally determined by the study of the projected surface of the initial droplet during the whole atomization process (more details can be found in refs. [8, 9]) and is well reproduced by the following relation (Eq. 4):

$$T_{ini} = 0.75 \cdot T \cdot We^{-0.06} \text{ with } T = \frac{D_0}{V} \cdot \sqrt{\frac{\rho_l}{\rho_g}} \tag{4}$$

The last parameter to take into account for complete characterization of the atomization process is the secondary droplets distribution (number and size of secondary fragments). This factor is very important because it determines the number and the size of the droplets created during the breakup process. This parameter has also been determined by Vieille. Simplified secondary distributions extracted from experimental results can be found in the following table (Table 1). These distributions give the number and the size of secondary droplets created by the fragmentation depending

	Percentage of parent droplet diameter		
Regime	10%	30%	50%
Bag breakup	2	2	1
Transitional breakup	3	1	1
Shear breakup	4	2	2

Table 1 Secondary droplet distributions

on the initial droplet diameter. The model constituted by transition, initiation time and distributions have been introduced in the THESEE code from SNECMA. This code is particularly dedicated to the simulation of phenomena encountered in rocket engines. For the droplet tracking, a lagrangian approach is considered.

2.2. Turbulent vaporization model

This model is based on the Birouk's experimental study [1]. In this experiment, a liquid fuel droplet is introduced into an isotropic and homogeneous turbulent flow without mean velocity. During the experiment the droplet diameter is tracked by a CCD camera. With this technique it was possible to obtain the following relation (Eq. 5) for the turbulent vaporization rate K:

$$\frac{K}{K_S} - 1 = 0.019 \cdot R_t^{2/3} \cdot Sc^2 \tag{5}$$

where K_S is the quasi-steady vaporization rate previously defined (Eq. 2), Re_t is the turbulent Reynolds number based on a turbulent length scale and Sc is the Schmidt number. Finally, the modeling of the turbulent vaporization is equivalent to the correction of the quasi-steady theory introducing turbulence effects. The turbulent vaporization model constituted by the turbulent vaporization rate correlation has been introduced in the MSD code from ONERA. This code is dedicated to the simulation of processes encountered in cryogenic rocket engines.

3. Conditions of computations

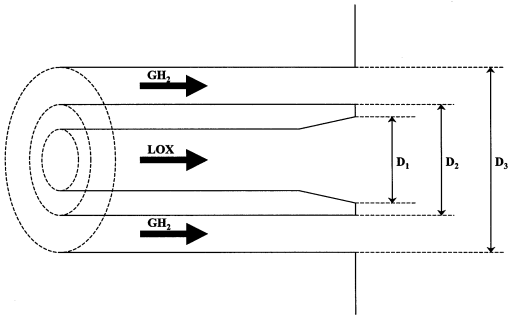

Figure 1 Configuration of the coaxial injector

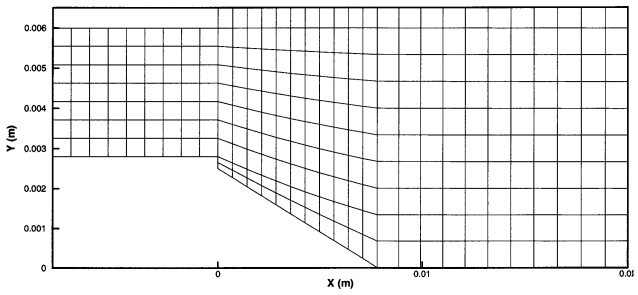

Figure 2 Meshing details of the LOX injection zone

The computational domain is identical to the MASCOTTE test bench operated by ONERA [5]. This experimental setup is dedicated to test a single cryogenic coaxial injector similar to those used in the Vulcain engine of the European launcher Ariane V. The configuration of the injector used in this numerical study is reproduced on figure 1, and dimensions are respectively 5, 5.6 and 12mm for D_1, D_2 and D_3. The computational domain is reproduced on figure 3. It is composed of 4223 hexaedral elements and its total length is 40cm. The liquid oxygen droplets are introduced in the

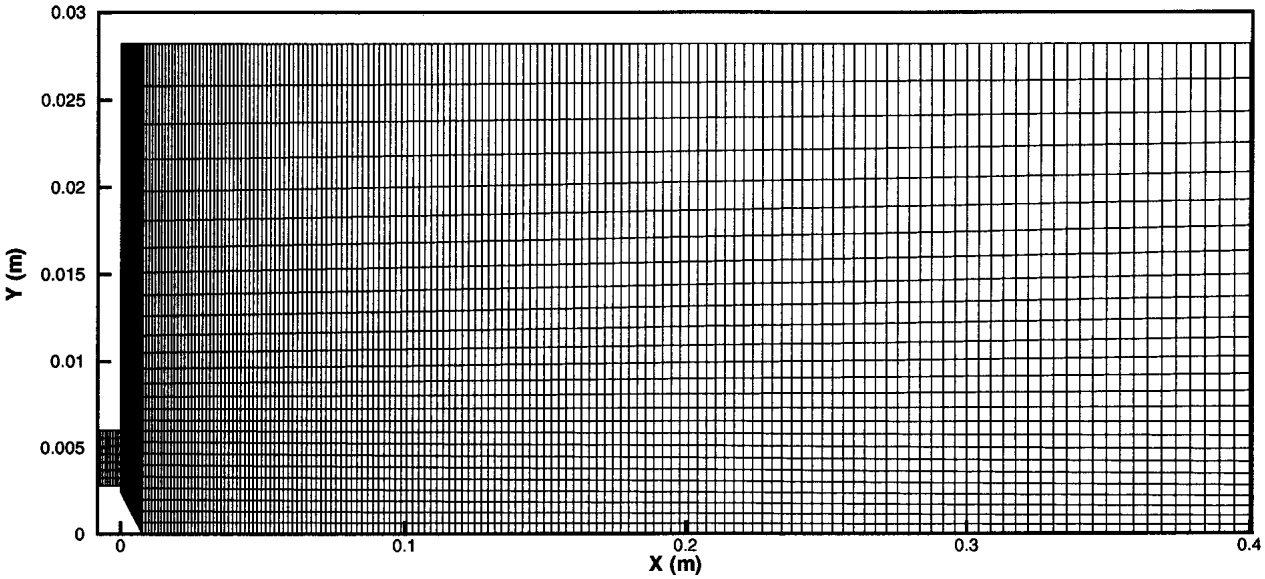

Figure 3 Computational domain

computational domain by the inner part of the injector on the surface of the potential cone (see Fig. 2). Initial conditions are the same for secondary atomization and turbulent vaporization computations and are summarized in table 2.

	LOX	GH_2
Pressure (MPa)	1.0	1.0
Temperatue (K)	85	287
Velocity (m/s)	2.18	319
Massflow (g/s)	50	23.7
Density (kg/m^3)	1170	0.84
Viscosity (kg/m/s)	1.94×10^{-4}	8.6×10^{-6}
Surface tension (N/m)	1.44×10^{-2}	–

Table 2 Initial conditions for computations

For secondary atomization, several initial droplet distributions have been considered. The first one is a Rosin-Rammler distribution (Eq. 6), where ν_c represents the droplet cumulative volume:

$$1-\nu_c\left(D\right)=\exp\left[-\left(D/D_{RR}\right)^N\right] \text{ with } N=2.25 \text{ and } D_{RR}=130\times10^{-6}m \tag{6}$$

The Sauter mean diameter of this distribution is D_{32RR}=82$\times10^{-6}$m, that is why a monodisperse distribution with diameter equal to D_{32RR} has also been considered. Three other monodisperse distributions have been used with initial diameter equal to 50$\times10^{-6}$, 100$\times10^{-6}$ and 150$\times10^{-6}$m. In the case of computations with the initial Rosin-Rammler distribution an additional computation have been performed without secondary atomization model. For all distributions considered in this study, the droplet injection angle depends on the insertion location (x) and follows the relation (7).

$$\theta\left(x\right)=\arctan\left[\frac{R_i\left(1-x/L_c\right)}{\left(x+R_i/\tan\theta_i\right)}\right] \text{ with } \tan\theta_i=0.68\left(U_{gas}/U_{liq}-1\right)\sqrt{\rho_g/\rho_l} \tag{7}$$

Finally, for the droplet initial velocity, the following relation (8) is used, where α is the cone angle and U_n is the normal velocity.

$$U_{drop0}=U_n/\cos\left(\pi/2-\alpha-\theta\right) \text{ with } U_n=0.66\text{m/s and } \alpha=17.7° \tag{8}$$

Initial droplets distribution	Droplet number
Rosin-Rammler (without atomization)	3259
Monodisperse 50×10^{-6}m (with atomization)	32934
Monodisperse 82×10^{-6}m (with atomization)	38549
Rosin-Rammler (with atomization)	37914
Monodisperse 100×10^{-6}m (with atomization)	36296
Monodisperse 150×10^{-6}m (with atomization)	36922

Table 3 Final droplets number

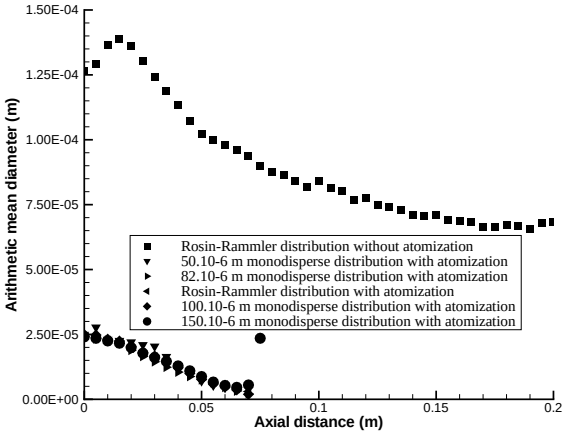

Figure 4 Axial variation of D_{10}

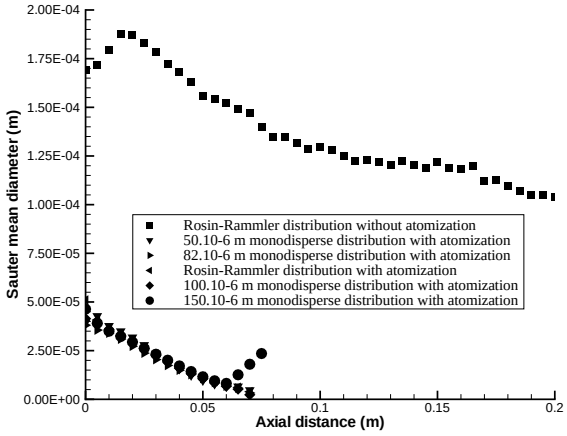

Figure 5 Axial variation of D_{32}

For turbulent vaporization, only the 82×10^{-6}m monodisperse distribution has been considered. All other injection properties (angle and velocity) are identical for secondary atomization and turbulent vaporization computations.

4. Results and discussion

4.1. Secondary atomization

Droplet number

The computations have been stop when the total droplet number stops to evoluate. Indeed, at the begining of computation, the total number of droplets increase because of injection and droplets atomization. After a certain time, an equilibrium between vaporization (diseapering) and atomization (creation) appears, and the total number of droplet is quasi constant. Table 3 gives the final droplet number for the different distributions considered. With this table, it is clear that the atomization process influences widely the final droplet number (about 10 times more droplets in the case of simulation with secondary atomization). In the case of computations with initial 50×10^{-6}m distribution the number of droplets is slightly lower than in other cases. This difference is due to the smaller size of droplets created. Indeed, during the breakup process, smaller droplets are generated with a criterion which is not sufficient to cause other fragmentations, limiting the number of droplets. For the larger initial distributions, the final droplet number is independant on initial distribution.

Droplet mean diameters

Figures 4 and 5 present the axial variation with distance from injection of droplet mean diameters D_{10} and D_{32}. These two parameters have been obtained by averaging over the whole calculation.

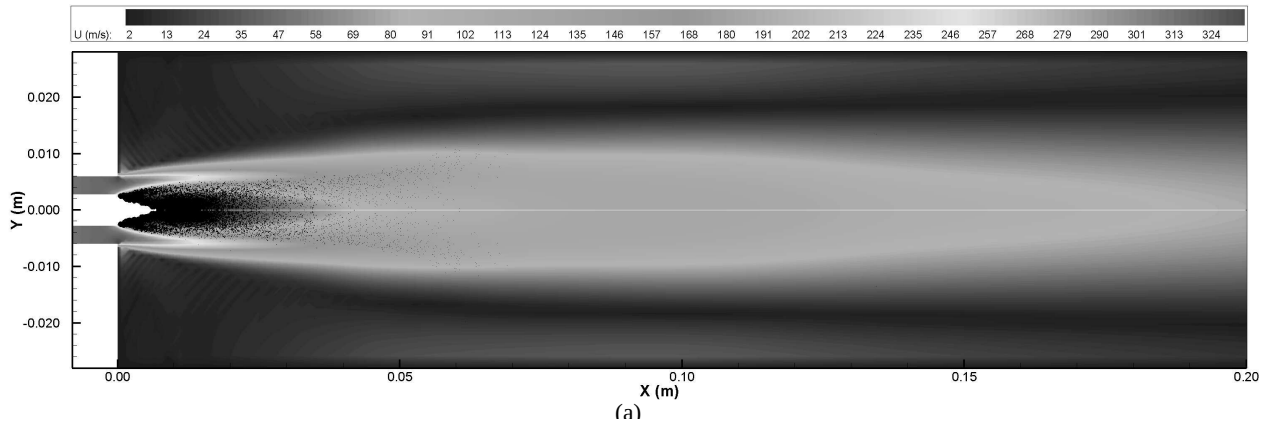

(a)

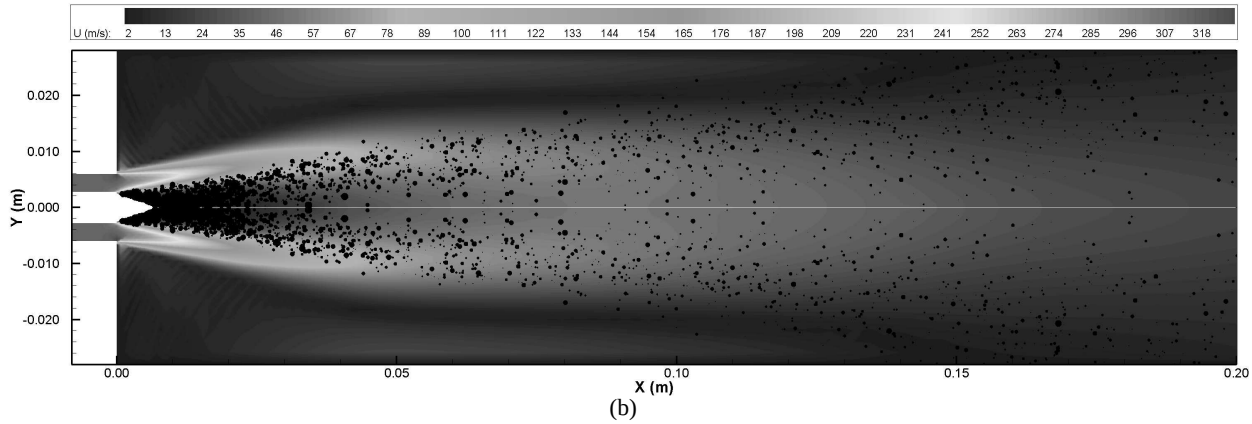

(b)

Figure 6 Superimposition of LOX droplet with mean velocity field;
(a) with atomization; (b) without atomization

Computations with secondary atomization give the same behavior for droplet mean diameters. This behavior is due to the rapid decreasing of the droplet size by the atomization process. In the case of computations without secondary atomization, the first increasing part of the curve is due to the rapid disappearing of the smallest droplets introduced in the computational domain. The last decreasing part of the curve corresponds to the partial vaporization of the biggest droplets reducing their diameters and therefore their mean diameters. With these figures it is clear that in the case of computations without secondary atomization, droplets continue to exist up to 20cm from the injection, whereas in the case of computations with secondary atomization there is no more liquid after a distance of about 7cm. This difference shows the importance of secondary atomization in spray formation and therefore two-phase combustion.

Spray length

For computations with the initial Rosin-Rammler distribution, superimpositions of the final spray with the mean velocity field are represented on figure 6. This figure shows the difference between the computations with and without secondary atomization. In the case of simulations with secondary atomization the spray length is much smaller than in the case of computations without secondary fragmentation. This difference is due to the rapid disappearing of smaller droplets created by fragmentation because of vaporization process. In the case of computations without secondary atomization, the vaporization process is not sufficient to cause the total disappearing of the biggest droplets.

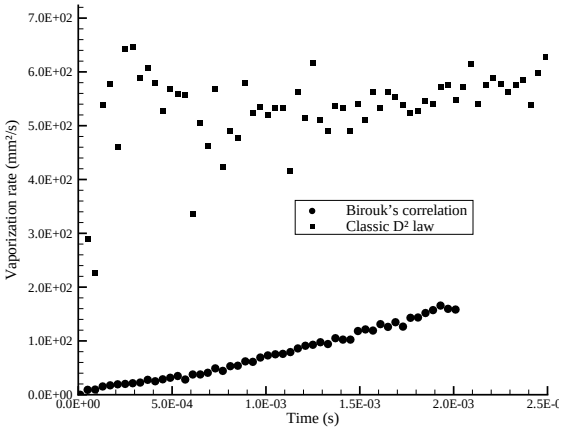

Figure 7 Temporal evolution of droplet vaporization rate

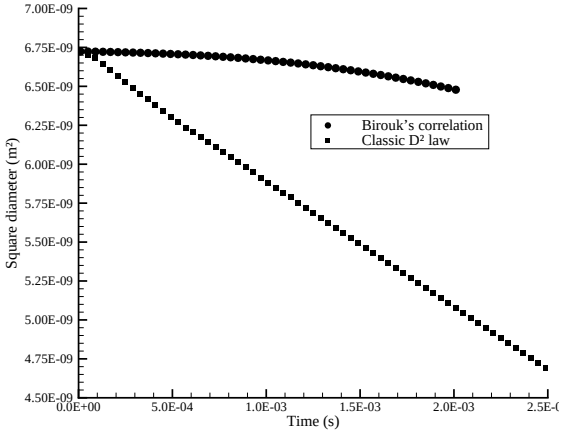

Figure 8 Temporal evolution of droplet square diameter

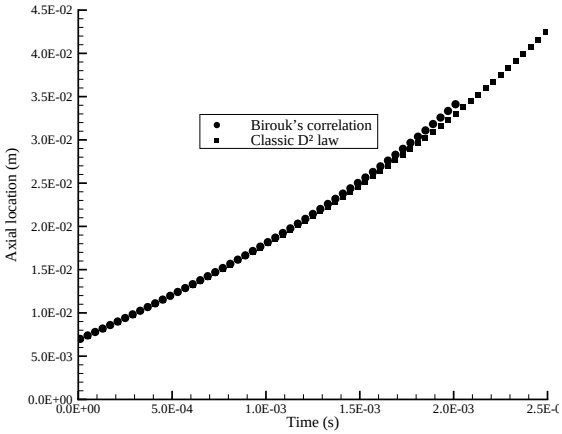

Figure 9 Temporal evolution of droplet axial location

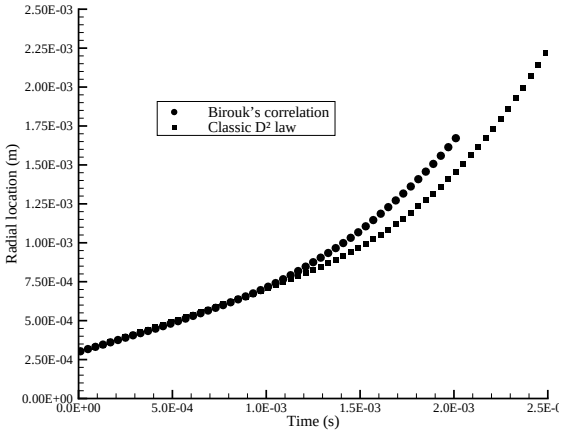

Figure 10 Temporal evolution of droplet radial location

4.2. Turbulent vaporization

Vaporization rate

Figure 7 presents the vaporization rate for computations with the classical D^2 law and the turbulent vaporization correlation. This figure highlights the importance of the turbulence in the vaporization process. Indeed, at the end of the computation ($t \approx 2.0 \times 10^{-3}$s) the ratio between turbulent vaporization rate and classical vaporization rate is about 3. The increasing of the classical vaporization rate is due to the droplet preheating by the ambient gas. In the case of computations with turbulent vaporization law no heating phase can be observed, resulting in a quasi constant turbulent vaporization rate during the whole calculation.

Droplet diameter

To permit comparison with the D^2 law previously presented (Eq. 2), the temporal evolutions of the droplet square diameter have been reproduced on figure 8. This figure shows a large difference between the classical D^2 law and the Birouk's law. Indeed, the decreasing of the diameter in the case of turbulent vaporization is much faster than in the case of standard D^2 law. The non linearity of the curve concerning the classical vaporization is due to the droplet heating.

Droplet location
Figures 9 and 10 show the droplet location during the vaporiation process. In the two cases (with turbulent vaporization law and classical D^2 law), the droplet location is the same during the main part of the computation which demonstrates the independence of the droplet location with vaporization process. The slight difference at the end of the simulation is due to the variation of the ambient gas properties because of the vapor generation by the vaporization process. For this point, more studies must be done. Indeed, the droplet drag coefficient is dependent on the surrounded gas properties, which is directly influenced by the droplet vaporization.

5. Conclusions

Secondary atomization and turbulent vaporization models based on experimental studies have been developped and used to compute a spray formation and its vaporization. In the case of secondary atomization, the spray length, number and size of droplets is widely dependent on the breakup process. The final droplet number is only slightly dependent on the initial droplet distribution and depends essentially on the size of initial droplets. In the case of turbulent vaporization computations, the vaporization rate and the decreasing of the droplet diameter is widely dependent on the turbulence of the ambient gas, whereas the droplet trajectory is only slightly influenced by the vaporization process. This particular point needs more studies.

Acknoledgements
This work was supported by the joint CNRS/CNES/SNECMA/ONERA program on “Combustion dans les moteurs fusées”. The computations concerning the THESEE code are perfomed with the support of CRIHAN. Emmanuel Bodèle is supported by a joint grant from ONERA/Conseil Régional du Centre.

References

[1] Birouk M. 1996 *PhD Thesis, University of Orléans*.
[2] Gelfand B. E. 1996 *Prog. Energy and Combust. Sci.* **22** 201–265.
[3] Godsave G. A. E. 1953 *Fourth Int. Symp. Comb.*
[4] Gökalp I., Chauveau C., Morin C., Vieille B. and Birouk M. 2000 *Atomization and Sprays* **10** 475–510.
[5] Habiballah M., Vingert L., Duthoit V. and Vuillermoz P. 1998 *J. Prop. Power* **14** 782–788.
[6] Shraiber A. A., Podvysotsky A. M. and Dubrovsky V. V. 1996 *Atomization and Sprays* **6** 667–692.
[7] Spalding D. B. 1953 *Fourth Int. Symp. Comb.*
[8] Vieille B. 1998 *PhD Thesis, University of Orléans*.
[9] Vieille B., Chauveau C. and Gökalp I. 1999 *16^{th} ILASS Conference*.